processes

MDPI

Article

Experimental Study on the Enhancement Mechanism of Multi-Component Thermal Fluid Huff-n-Puff in Deep Extra-Heavy Oil Reservoirs

Rui Han [1,2], Tao Lin [1,2], Jianliang Zhang [1,2], Rong Sun [2,3], Zhongtao Yuan [2,3], Ming Wang [2,3], Lan Mo [2,3], Xiaopu Wang [4,*], Hailong Zhao [4], Bingbing Liu [4] and Zhaoxu Zhang [4]

1 National Key Laboratory for Efficient Development of Offshore Oil and Gas, Tianjin 300459, China; lintaodqpi@163.com (T.L.)
2 Key Laboratory of Offshore Heavy Oil Thermal Recovery, China National Offshore Oil Corporation Limited, Tianjin 300459, China; 15932563309@163.com (R.S.); 18829513027@163.com (Z.Y.); seasky517@126.com (M.W.); tanxixixi9999@gmail.com (L.M.)
3 China Oilfield Services Limited, Tianjin 300459, China
4 School of Petroleum Engineering, China University of Petroleum (East China), Qingdao 266580, China; upczhaohailong@126.com (H.Z.); z24020046@s.upc.edu.cn (B.L.); zhangzhaoxu22@163.com (Z.Z.)
* Correspondence: wxp@upc.edu.cn

Abstract

Due to high formation pressure and extremely poor crude oil mobility, the synergistic enhancement mechanism of heat–gas–chemical interactions and the governing laws of key factors during multi-component thermal fluid (MCTF) huff-n-puff in deep extra-heavy oil reservoirs remain unclear. In this study, a one-dimensional sand pack model was used to systematically conduct MCTF huff-n-puff depletion production experiments under a high pressure of 30 MPa, complemented by viscosity–temperature tests, PVT dissolution viscosity reduction tests, and viscosity reducer concentration–viscosity tests. A single-factor analysis approach was employed to investigate the effects of injection temperature, gas medium type, gas–oil ratio (GOR), and viscosity reducer concentration on the huff-n-puff recovery factor. Based on the single-factor tests and the nine-run L9 orthogonal experiments, the results show that injection temperature is the primary controlling factor: the low-pressure stage (2 MPa) recovery factor of CO_2 rises from 15.9% to 18.7% as the temperature increases from 90 °C to 120 °C, and further to 19.6% at 150 °C; 120 °C is identified as the preferred injection temperature under the studied conditions. Owing to its higher solubility (114.9 m^3/m^3) and solution gas drive energy, CO_2 outperforms CH_4 and flue gas, delivering a recovery factor 3 percentage points higher than that of CH_4 and 18 percentage points higher than that of flue gas. The recovery factor increased monotonically with GOR over the tested range of 10–30, and no gas channeling was observed. The recovery benefit of the viscosity reducer increases markedly as the concentration rises from 1 to 5 wt%, whereas the incremental gain beyond 5 wt% becomes marginal. Run 4 (120 °C + CO_2 + GOR 20 + 5 wt% viscosity reducer) achieved the highest total recovery factor of 44.6% among the nine orthogonal combinations, representing the best-performing combination within the L9 design rather than a verified global optimum. The grey relational ranking of the four factors is injection temperature > viscosity reducer concentration > gas type > GOR. The findings provide an experimental basis, under the tested Shengli extra-heavy oil system and the present 30 MPa one-dimensional sand pack conditions, for optimizing MCTF huff-n-puff process parameters in deep extra-heavy oil reservoirs.

Check for updates

Academic Editor: Federica Raganati

Received: 1 August 2026
Revised: 20 September 2026
Accepted: 8 October 2026
Published: 3 November 2026

Copyright: © 2026 by the authors. Licensee MDPI, Basel, Switzerland. This article is an open access article distributed under the terms and conditions of the Creative Commons Attribution (CC BY) license.

Keywords: deep extra-heavy oil; multi-component thermal fluid; one-dimensional sand pack; depletion production; flow–drive balance; enhancement mechanism

1. Introduction

Deep extra-heavy oil resources (burial depth > 2000 m, formation crude oil viscosity > 50,000 mPa·s; classification per the Chinese heavy-oil standard [1]) account for a considerable proportion of global oil and gas resources, but their exploitation faces extreme technical challenges. At reservoir temperature (80–100 °C), the crude oil viscosity can reach tens of thousands to hundreds of thousands of mPa·s [2,3], leaving the oil virtually without natural flow capability. Moreover, deep high-temperature and high-pressure conditions cause severe wellbore heat loss and rapid steam quality decay, making it difficult for conventional cyclic steam stimulation to establish an effective displacement pressure differential and resulting in very poor development performance. Therefore, achieving effective production of extra-heavy oil under deep reservoir conditions is a critical challenge that urgently needs to be addressed in heavy oil recovery. The viscosity threshold of extra-heavy oil (>50,000 mPa·s) follows the Chinese heavy oil classification standard [1], while the depth threshold corresponds to the development scheme of the target reservoir.

To overcome these bottlenecks, heavy oil recovery technologies have been developed along three main routes: thermal recovery, gas injection, and chemical assistance. With respect to thermal recovery, temperature is regarded as the key variable controlling extra-heavy oil mobility, and the crude oil viscosity can decrease by two to three orders of magnitude over 90–150 °C [4]; cyclic steam stimulation has been widely practiced in onshore blocks such as Liaohe [5] and offshore heavy oil fields [6], and gas-assisted variants—such as N_2-assisted cyclic steam stimulation [7] and CO_2/N_2 injection during steam injection [8]—as well as EOR methods after steam injection [9] have been continuously developed. With respect to gas injection, numerous studies have demonstrated that the dissolution-induced viscosity reduction and swelling-driven energy augmentation of CO_2 constitute the core mechanism of huff-n-puff stimulation [10–13]; CO_2 flooding and storage has accordingly developed into a mature technology system [13]; in contrast, the solubility of CH_4 in heavy oil is only about one-third of that of CO_2, and the interfacial behavior of CO_2–solvent–heavy oil systems further differentiates the gas performance [12,14]. With respect to chemical assistance, viscosity reducers (especially anionic–nonionic composite surfactants) can substantially lower the apparent viscosity of extra-heavy oil through dispersion and interfacial regulation [15,16]; combined thermal–gas–chemical processes—such as CO_2 and viscosity breaker-assisted steam huff-n-puff in horizontal wells [17], HDCS technology for super-heavy oil [18], oil-soluble viscosity reducer with CO_2-assisted steam flooding [19], and CO_2–chemical synergetic heat transfer [20], which have extended the chemical route, together with surfactant-assisted steam processes [21,22], thermochemical techniques [23,24], and foam anti-channeling in CO_2 flooding [25]—have progressively moved toward the coupling of thermal, gas, and chemical effects.

At the mechanism level, molecular simulation has been introduced into oilfield chemistry and enhanced oil recovery research [26–28]; molecular dynamics studies of heavy oil in supercritical water and multi-component thermal fluids [29] and of hybrid CO_2–thermal systems [30] have deepened the understanding of steam–gas–chemical coupling and supported the development of multi-component thermal fluid (MCTF) technology for offshore and onshore heavy oil reservoirs [6,29,30]. Under primary pressure depletion, foamy oil behavior and depletion-rate effects have been shown to govern the solution gas drive of

heavy oils [31–34]; these studies established the classical interplay between oil flow capacity and driving energy on which the present interpretation builds.

However, most of these studies were conducted under single-factor or two-factor conditions, using different experimental apparatus, crude oils, and pressure regimes, which limits the cross-study comparability of the reported results; the relative importance of different factors for the recovery factor remains unclear; the synergistic enhancement mechanism among thermal, gas, and chemical effects lacks quantitative characterization; and the optimal parameter ranges and the interactions among factors remain insufficiently quantified. Existing studies therefore provide limited quantitative guidance for the selection of field process parameters.

To address these gaps, this study tests the following hypothesis: under deep high-pressure conditions, the huff-n-puff recovery factor is jointly governed by the crude oil flow capacity and the solution gas driving force, and the four key factors (injection temperature, gas type, GOR, and viscosity reducer concentration) act on these two dimensions with different weights and interact with one another. Accordingly, a systematic experimental investigation of MCTF huff-n-puff depletion production was carried out under a deep reservoir pressure of 30 MPa using a one-dimensional sand pack high-pressure displacement apparatus, combining single-factor tests with an L9(3^4) orthogonal design and grey relational analysis [35,36]. Compared with previous studies, the contributions of this work are threefold: (1) a full-process single-factor analysis of the four factors was completed on a unified experimental platform, improving the cross-system consistency of the four-factor comparison; (2) grey relational analysis was used to rank the four factors by grey relational degree, complemented by an L9(3^4) orthogonal design for multi-factor combination testing under unified conditions—the orthogonal design supports factor screening and ranking but does not by itself permit quantitative separation of factor interactions, which would require additional controlled runs; and (3) the experimental data characterized the differentiated roles of the three components and provided an experimental reference for process parameter optimization; the quantitative conclusions of this work are specific to the tested Shengli extra-heavy oil system under the present 30 MPa one-dimensional sand pack conditions.

2. Materials and Methods

2.1. Experimental Apparatus

The Schematic of the experimental apparatus is listed in Figure 1.The intermediate container (Haian Petroleum Scientific Research Instrument Co., Ltd., Haian, Jiangsu, China) has a pressure rating of 0–50 MPa and a maximum temperature rating of 200 °C. The opening error of the back-pressure regulator (Haian Petroleum Scientific Research Instrument Co., Ltd., Haian, Jiangsu, China) is less than 0.05 MPa. In huff-n-puff mode, injection and production were alternately performed through the same port of the sand pack model. (Haian Petroleum Scientific Research Instrument Co., Ltd., Haian, Jiangsu, China) The thermal component of the MCTF was injected as hot water preheated to the target temperature; at 30 MPa, water at the studied temperatures remains in the compressed liquid state rather than as steam.

2.2. Experimental Materials

(1) Basic physical properties of the sand pack

After sand packing, the measured physical properties are listed in Table 1. Quartz sand was used for packing. The initial irreducible water saturation was 14.2% and the initial oil saturation was 85.8%, providing a unified reference baseline for all experimental groups.

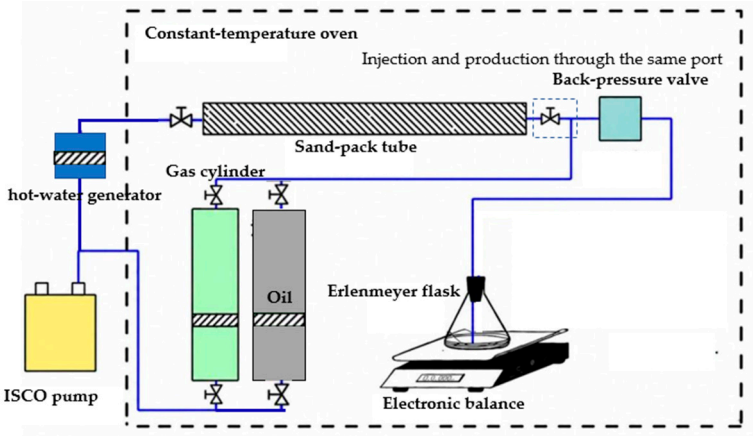


Figure 1. Schematic of the experimental apparatus.

Table 1. Basic physical parameters of the sand pack.

Parameter	Value
Length (cm)	60
Diameter (cm)	2.5
Permeability ($\times 10^{-3}$ μm^2)	50
Porosity (%)	32.5
Initial oil saturation (%)	85.8
Irreducible water saturation (%)	14.2
Maximum working pressure (MPa)	40
Maximum working temperature (°C)	350

(2) Experimental crude oil

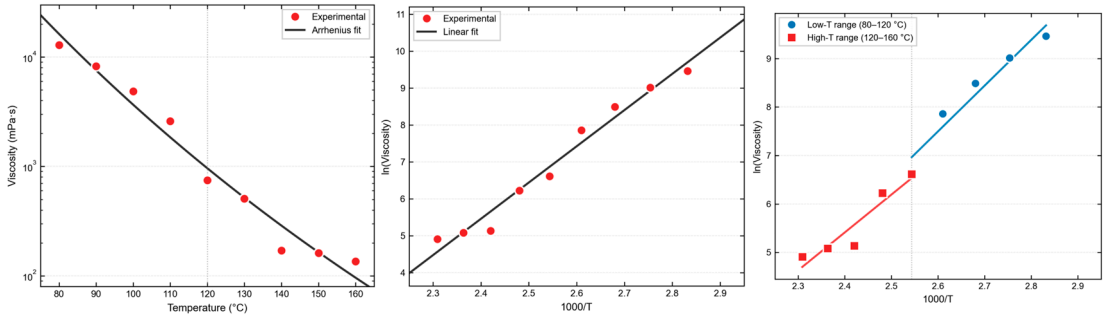
The experimental oil was dehydrated and degassed crude oil taken from a typical ultra-heavy oil block of the Shengli Oilfield (degassed oil viscosity > 100,000 mPa·s at reservoir temperature) [37]; its basic properties are listed in Table 2. The crude oil viscosity is 8.0×10^3 mPa·s at 90 °C, 7.8×10^2 mPa·s at 120 °C, and 161.54 mPa·s at 150 °C, consistent with the viscosity–temperature curve in Figure 2 (12,869 mPa·s at 80 °C). The viscosity–temperature curve indicates that 90–150 °C is the "temperature-sensitive window", within which the crude oil viscosity decreases sharply—for every 30 °C increase, the viscosity drops by about one to two orders of magnitude. This viscosity–temperature characteristic forms the physical basis for selecting temperature as the principal factor in this study.

Table 2. Basic properties of the experimental crude oil.

Property	Value
Density at 20 °C (g·cm^{-3})	0.9786
Viscosity at 90 °C (mPa·s)	8.0×10^3
Viscosity at 120 °C (mPa·s)	7.8×10^2
Viscosity at 150 °C (mPa·s)	161.54
Average molecular weight (g·mol^{-1})	583
Saturates content (%)	32.6

Table 2. *Cont.*

Property	Value
Aromatics content (%)	30.4
Resins content (%)	25.8
Asphaltenes content (%)	11.2
Acid number (mg KOH·g^{-1})	3.62



(**a**) (**b**) (**c**)

Figure 2. Crude oil viscosity–temperature characteristics and Arrhenius fitting. (**a**) Viscosity–temperature curve (semi-log scale), with 120 °C as the rheological inflection point. (**b**) Arrhenius linearized fitting, activation energy Ea = 81.6 kJ/mol. (**c**) Piecewise Arrhenius fitting, low-temperature segment Ea = 78.5 kJ/mol, high-temperature segment Ea = 64.9 kJ/mol.

(3) Experimental gases

CO_2: industrial grade, purity ≥ 99.9%. CH_4: high-purity methane, purity ≥ 99.99%. Flue gas: simulated industrial flue gas, formulated by volume as N_2 83% + CO_2 15% + O_2 2%.

(4) Viscosity reducer

An anionic surfactant—C11 alkylbenzene sulfonate viscosity reducer—was used. It is a brownish-yellow viscous liquid of analytical reagent grade (purity ≥ 99.7%). Prior to each test, the viscosity reducer product was loaded at a dosage amounting to the target mass fraction (1, 3, 5, or 10 wt% in the single-factor tests; 0, 3, or 5 wt% in the L9 design) of the crude oil saturated in the sand pack (approximately 80 g; e.g., approximately 4.0 g of product at 5 wt%). The product is oil-soluble and immiscible with water: in the intermediate container it formed a separate layer above the hot water, with the experimental gas above it. For the 0 wt% groups, no viscosity reducer was added. The viscosity reducer exhibits good thermal stability at 90–150 °C (the viscosity reduction retention rate after high-temperature aging for 72 h exceeds 85%).

2.3. Experimental Design

A single-factor analysis strategy was adopted to investigate, in turn, the effects of the four factors on the huff-n-puff recovery factor. Within each experimental group, only the target factor was varied while the remaining conditions were held at the group-specific reference condition: the gas type experiments were conducted at 120 °C and GOR 30; the temperature experiments at GOR 20 with 5 wt% viscosity reducer; the GOR experiments at 120 °C with 5 wt% viscosity reducer; and the viscosity reducer experiments at 90 °C and GOR 30, with CO_2 as the reference gas and a soak time of 24 h in all groups. Throughout this study, the gas–oil ratio (GOR) is defined as the volume of injected gas under standard conditions (0 °C, 101.325 kPa) per unit volume of crude oil. The injected gas volume at each GOR level was determined by multiplying the crude oil volume saturated in the sand pack

by the corresponding GOR value; that volume of gas was then injected under standard conditions (0 °C, 101.325 kPa), i.e., GOR values of 10, 20, and 30 correspond to injecting 10, 20, and 30 times the oil volume of gas, respectively. The levels of each factor were injection temperature 90/120/150 °C; gas type CO_2/CH_4/flue gas; GOR 10/20/30; and viscosity reducer concentration 1–10 wt% for the single-factor groups (levels 1, 3, 5, and 10 wt%) and 0/3/5 wt% in the L9 orthogonal design.

The experimental procedure is as follows:

① The prepared quartz sand was packed into the one-dimensional sand pack tube, evacuated and saturated with water, and the absorbed water volume was recorded. The permeability was then measured by water flooding. The thermostatic system was turned on, and the core holder and fluid containers were heated to the set experimental temperature and stabilized for 1 h.

② Using the group-specific reference condition (120 °C, GOR 30, and 0 wt% viscosity reducer), experiments were conducted under a depletion production mode for each of the three gas compositions. An ISCO positive displacement pump was used to inject the prepared oil sample into the sand pack core at a fixed flow rate of 0.01 mL·min^{-1} until saturation was reached.

In each huff-n-puff cycle, the MCTF was injected through the same port of the sand pack model after oil saturation. The intermediate container was charged—in this order from bottom to top—with hot water preheated to the target injection temperature (at 30 MPa it remains in the compressed liquid state rather than as steam), the calculated viscosity reducer dosage defined in Section 2.2 (4), and the experimental gas; because the viscosity reducer is oil-soluble and immiscible with water, it formed a distinct layer between the water and the gas. During injection, the viscosity reducer and the gas entered the sand pack first, driven by the hot water below them; after the entire gas charge—set by the GOR, i.e., the GOR value multiplied by the crude oil volume saturated in the sand pack (both expressed at the surface standard conditions of 0 °C and 101.325 kPa)—and the entire reducer dosage had entered, the core pressure had not yet reached 30 MPa, and hot water injection was therefore continued to raise the core pressure to 30 MPa, after which the valves were closed and the soak stage began. The gas charge and the reducer dosage were the independently set variables (fixed by the GOR and the target concentration, respectively), so that only the target factor (temperature, gas type, GOR, or viscosity reducer concentration) varied among the groups; the hot water volume was the make-up amount required to reach the 30 MPa target, approximately 10 mL in each run. For the 0 wt% groups, no viscosity reducer was added. The nominal saturated oil volume of each run is approximately 82 mL; the injected gas volumes at GOR 10, 20, and 30 are 0.82, 1.64, and 2.46 L under the surface standard conditions, respectively; and the hot water volume averaged approximately 10 mL per run (Supplementary Table S1).

③ Upon completion of injection, the valves at both ends of the core were closed immediately to start the soak stage (set to 24 h to ensure that heat, gas, and chemical agents fully interact and diffuse with the crude oil).

④ After the soak, the core outlet valve was opened to start production. The outlet end was connected to an oil collection device and pressure-monitoring equipment. The depletion was pressure-controlled by the back-pressure regulator alone (opening error < 0.05 MPa): the regulator set pressure was lowered gradually from the initial 30 MPa to the terminal 2 MPa. A rate-specified, pump-controlled pressure decline program was not used, and the detailed pressure–time schedule of each run was not systematically recorded. The produced liquid was collected at fixed time intervals, and the oil production rate and water cut were measured, until the outlet produced no oil or the pressure and flow rate remained stable for

1 h, at which point production was terminated. Pressure, flow rate, and production data throughout the injection–soak–production cycle were recorded.

⑤ Steps ①–④ were repeated with the injected gas replaced in turn by CH_4 and flue gas, so as to repeat the huff-n-puff experiments and ensure that the sole variable was the gas composition, thereby allowing for an accurate comparison of the differences among gases in huff-n-puff recovery performance.

⑥ Variable-temperature experiments: with the gas type varied among CO_2, CH_4, and flue gas while the gas–liquid ratio, injection volume, and soak time were held constant, the MCTF temperature was adjusted to 120 °C and 150 °C, respectively, and the above injection–soak–production cycles and data recording were repeated. A fresh core was used for each temperature level to ensure consistency of the initial saturation state and experimental conditions; the same fresh pack practice was applied to all the other experimental groups.

⑦ Variable-GOR experiments: with gas composition (the same gas selected in the variable-temperature experiments), temperature (120 °C), viscosity reducer concentration (5 wt%, the same baseline as the variable-temperature experiments), and soak time held constant, the gas–oil ratio was adjusted to 10, 20, and 30, respectively, and the above huff-n-puff production operations were repeated.

It should be noted that all experiments reported in this study were single-run tests performed on fresh sand packs. No replicate runs were performed, so no standard deviations or error ranges are available; the reported recovery factors represent trends observed in individual experimental runs, and differences of a few percentage points among conditions should be interpreted as observed trends rather than statistically established differences. Replicate experiments and error analyses for the key comparison conditions (temperature, GOR, viscosity reducer concentration, and the best-performing combination) are planned as subsequent work. In total, 32 independent fresh pack runs were conducted in five series: 3 gas-type runs (120 °C, GOR 30, 0 wt%), 9 temperature runs (GOR 20, 5 wt%), 9 GOR runs (120 °C, 5 wt%), 4 viscosity reducer concentration runs (90 °C, GOR 30, CO_2), and the 9 L9 orthogonal runs; the run at 120 °C + CO_2 + GOR 20 + 5 wt% is common to the temperature, GOR, and L9 series. The complete run-by-run listing, including the oil, gas, and hot water volumes of every run, is provided in Supplementary Table S1.

3. Results and Discussion

3.1. Influence Law of Multi-Component Thermal Fluid on Crude Oil Viscosity

The viscosity–temperature characteristics of crude oil constitute the physical basis of the temperature-dominated effect. The viscosity–temperature curve of the experimental crude oil in the range of 80–160 °C (Figure 2) indicates that when the temperature rises from 80 °C to 150 °C, the crude oil viscosity decreases from 12,869 mPa·s to 161.54 mPa·s, a reduction of 98.7%. The Arrhenius equation $\mu = A \cdot \exp(Ea/RT)$ was used to fit the viscosity–temperature data, yielding a global activation energy Ea = 81.6 kJ/mol ($R^2 = 0.972$). Piecewise fitting further reveals that 120 °C is the rheological inflection point: the low-temperature segment (80–120 °C) has an activation energy of 78.5 kJ/mol ($R^2 = 0.938$), while the high-temperature segment (120–160 °C) sees the activation energy drop to 64.9 kJ/mol ($R^2 = 0.884$). The decrease in activation energy is attributed to the disruption of π–π stacking and van der Waals forces between asphaltene–resin molecules by high temperatures, causing the crude oil to exhibit lower temperature sensitivity in the high-temperature segment. The existence of this inflection point provides a property-level basis for selecting 120 °C as the preferred injection temperature within the investigated range; beyond this temperature, the marginal recovery benefit of further heating diminishes.

The differences in PVT properties of the three experimental gases at 120 °C (Figure 3) constitute the microscopic mechanism by which gas type affects the recovery factor.

At 30 MPa, the solubility of CO_2 reaches 114.9 m^3/m^3, which is 1.8 times that of CH_4 (63.2 m^3/m^3) and 3.0 times that of flue gas (38.9 m^3/m^3). Correspondingly, CO_2 reduces the mixed oil viscosity from 780 mPa·s to 18.66 mPa·s (a viscosity reduction rate of 97.6%) at 30 MPa and 120 °C, whereas CH_4 only reduces it to 659.1 mPa·s (a reduction rate of 15.5%), and flue gas reduces it to 700 mPa·s (a reduction rate of 10.3%). The superior performance of CO_2 stems from its smaller molecular kinetic diameter (0.33 nm vs. 0.38 nm for CH_4) and the polar interactions brought by its quadrupole moment, making it easier to insert between asphaltene–resin lamellae. Therefore, CO_2 has the strongest dissolution viscosity reduction and energy augmentation potential among the three gases and is the optimal gas medium for multi-component thermal fluid.

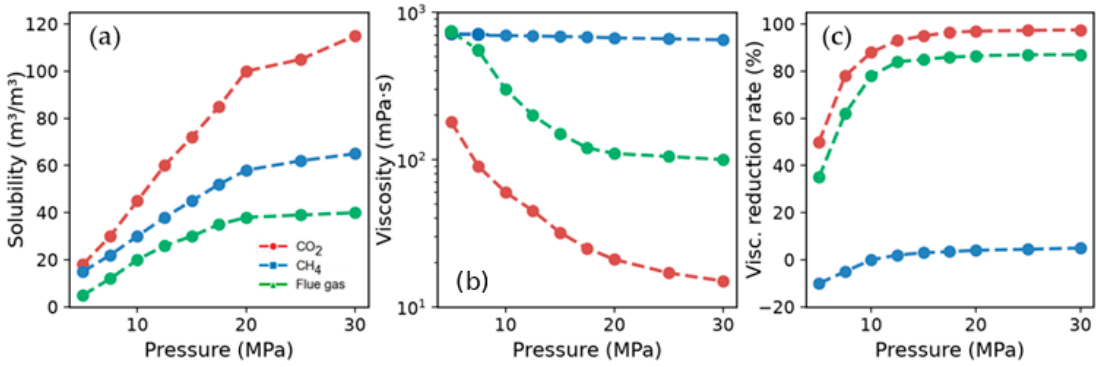


Figure 3. PVT properties of the three gases (120 °C). (**a**) Solubility vs. pressure; (**b**) mixed oil viscosity vs. pressure (semi-log scale); (**c**) viscosity reduction rate vs. pressure. At 30 MPa, CO_2 solubility reaches 114.9 m^3/m^3 with a viscosity reduction rate > 97%.

3.2. Recovery Characteristics of MCTF Pressure Depletion Huff-n-Puff

Physical Nature of the Pressure Depletion Huff-n-Puff Process

The complete MCTF huff-n-puff process consists of three stages: "injection–soak–pressure-depletion production". In the first two stages, the MCTF simultaneously modifies the crude oil properties and the reservoir energy state through mechanisms such as heating, gas dissolution, and chemical viscosity reduction; in the depletion production stage, the final huff-n-puff recovery factor is jointly determined by the crude oil flow capacity and the solution gas driving force. The crude oil flow capacity is governed by the combined viscosity reduction effect of thermal, chemical, and dissolved gas mechanisms, and controls whether the crude oil can flow within the pore network; the solution gas driving force is jointly determined by the amount of dissolved gas and the expansion ratio during depletion and determines whether the crude oil in the pores can be fully displaced and ultimately flow toward the wellbore.

To separate the relative contributions of the two, this study decomposes the depletion production process into two stages according to the pressure level and analyzes them separately. The high-pressure stage (from 30 MPa down to about 10 MPa) lies above the 10 MPa operational pressure boundary (set by the bottomhole operating pressure scheduled in the development plan of the target reservoir; the actual bubble-point pressures of the three gas systems were not measured), in which gas liberation is limited and elastic drive dominates. The recovery factor in this stage mainly reflects the elastic component of the driving energy. The low-pressure stage (from 10 MPa down to about 2 MPa) lies below this operational boundary, in which dissolved gas is liberated in large quantities and solution gas drive dominates. This stage is the dominant production period of huff-n-puff, and its recovery factor is jointly controlled by the flow capacity and the solution gas driving

force. This two-stage decomposition provides an experimental basis for the subsequent factor analysis.

3.3. Key Factors and Influence Patterns of Pressure Depletion Recovery

Building on the two-stage decomposition established in Section 3.2, this section examines in turn the influence of four factors—gas type, injection temperature, gas–oil ratio, and viscosity reducer concentration—on the huff-n-puff recovery factor. Within each experimental group, only the target factor was varied, while all other conditions were held constant.

3.3.1. Effect of Gas Type on Recovery

Under the conditions of temperature 120 °C, GOR 30, and viscosity reducer concentration 0 wt%, the huff-n-puff recovery factors of three gases—CO_2, CH_4, and flue gas—were tested, and the production process was metered separately by the high-pressure stage (10 MPa) and the low-pressure stage (2 MPa).

Figure 4 shows the recovery factors of the three gases in different pressure stages. As can be seen from Figure 4, in the low-pressure stage CO_2 achieves the highest recovery, followed by CH_4, with flue gas the lowest at only 8.8%; in the high-pressure stage, the recovery factors of CO_2 and CH_4 are relatively close, while flue gas produces almost no oil. Overall, the recovery factor of CO_2 is consistently higher than those of CH_4 and flue gas.

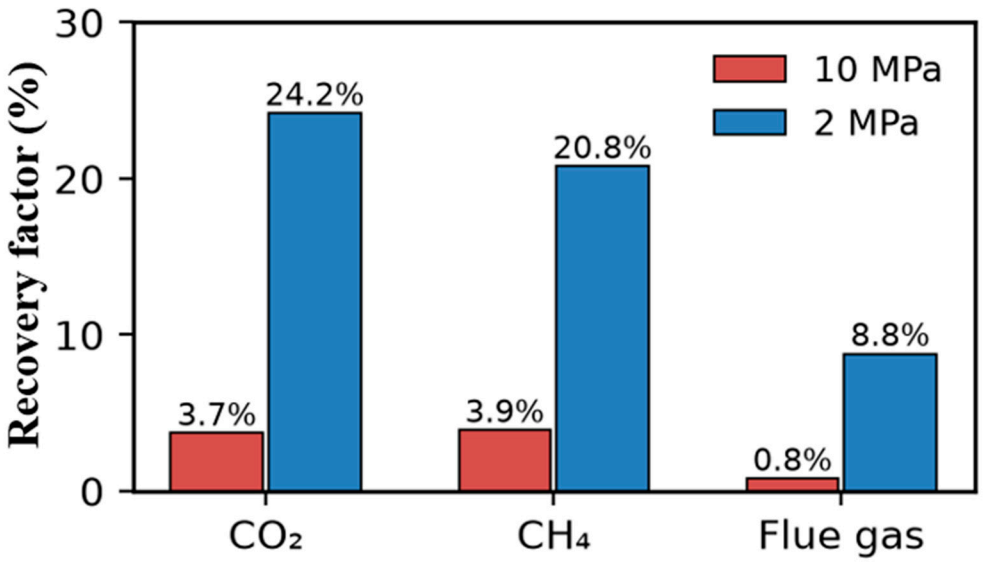


Figure 4. Effect of different gases on the recovery factor.

The differences in huff-n-puff performance among the three gases originate mainly from their different solubilities in crude oil. At 30 MPa and 120 °C, the solubility of CO_2 reaches 114.9 m^3/m^3, which is 1.8 times that of CH_4 (63.2 m^3/m^3) and 3.0 times that of flue gas (38.9 m^3/m^3). During the soak stage, a large amount of CO_2 dissolves in the crude oil, reducing the mixed oil viscosity from 780 mPa·s to 18.66 mPa·s (a 97.6% reduction); during the depletion stage, the dissolved CO_2 is liberated and expands violently, generating a strong solution gas driving force that displaces the crude oil out of the pores. CH_4, with lower solubility, achieves a viscosity reduction of 15.5%; flue gas, dominated by N_2, has even lower solubility with a viscosity reduction of 10.3%, so both exhibit recovery factors far below that of CO_2.

It can therefore be concluded that CO_2—with its advantages in both dissolution viscosity reduction and solution gas driving force—is the preferred gas medium for MCTF huff-n-puff. Where CO_2 supply is limited, flue gas can serve as an alternative medium;

however, under the tested conditions its low-pressure stage recovery factor (8.8%) was only about one-third of that of CO_2 (Figure 4), and the matching adjustments of injection parameters (temperature, GOR, and viscosity reducer dosage) required for field application would be substantial. These adjustments are left for subsequent work.

3.3.2. Effect of Temperature on Recovery

Under the conditions of GOR 20 and viscosity reducer concentration 5 wt%, the variations of the low-pressure stage (2 MPa) huff-n-puff recovery factor with temperature were tested for CO_2, CH_4, and flue gas at 90, 120, and 150 °C.

Figure 5 shows the relationship between the recovery factor of the three gases in the low-pressure stage (2 MPa) and temperature. As can be seen from Figure 5, as the temperature increases from 90 °C to 150 °C, the recovery factors of all three gases increase, but the magnitude of increase differs markedly across temperature ranges. In the range of 90–120 °C, the recovery factor of CO_2 rises from 15.9% to 18.7% (an increase of 2.8 percentage points); in the range of 120–150 °C, it further increases to 19.6% (an increase of 0.9 percentage points). The recovery factors of CH_4 and flue gas increase more modestly with temperature.

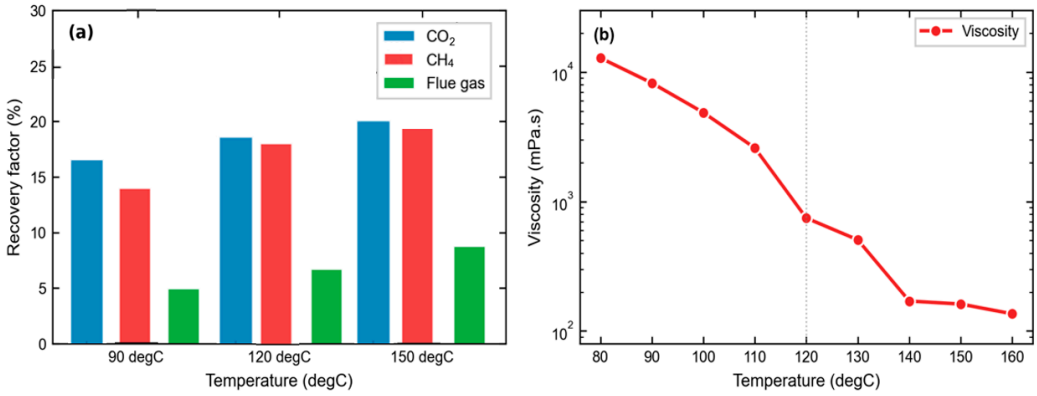


Figure 5. Effect of temperature on the low-pressure stage (2 MPa) recovery factor and crude oil viscosity–temperature characteristics. (**a**) Low-pressure stage recovery factors of the three gases at 90/120/150 °C, with CO_2 reaching 19.6% at 150 °C; (**b**) crude oil viscosity as a function of temperature (semi-log scale), with the dashed line at 120 °C indicating the rheological inflection point.

The effect of temperature on the recovery factor operates through two pathways. On the one hand, an increase in temperature substantially reduces the crude oil viscosity—from 8.0×10^3 mPa·s at 90 °C to 7.8×10^2 mPa·s at 120 °C (≈90% reduction)—thereby improving oil-phase mobility; at the same time, the temperature rise enhances the diffusion capacity of CO_2 molecules, enabling them to dissolve more thoroughly in the crude oil. On the other hand, a temperature increase reduces the solubility of gases in crude oil—for every 30 °C increase, the solubility of CO_2 decreases by about 10–15%—thereby weakening the solution gas driving force in the low-pressure stage. In the 90–120 °C range, the mobility improvement brought about by the viscosity reduction dominates, and the recovery factor rises rapidly; in the 120–150 °C range, the mobility improvement approaches saturation (residual oil saturation becomes the new limiting factor), while the side effect of reduced gas solubility becomes obvious, slowing the rate of recovery growth.

Within the studied range, the recovery gain beyond 120 °C diminishes while energy consumption keeps rising; 120 °C is therefore regarded as the preferred injection temperature under the tested Shengli extra-heavy oil system and the present 30 MPa one-dimensional sand pack conditions, although a dedicated energy consumption analysis was beyond the scope of this study.

3.3.3. Effect of Gas–Oil Ratio on Recovery

Under the conditions of 120 °C and 5 wt% viscosity reducer concentration (the same baseline as the variable-temperature experiments), the variations of the low-pressure stage (2 MPa) huff-n-puff recovery factor with GOR were tested for the three gases at GORs of 10, 20, and 30.

Figure 6 shows the low-pressure stage (2 MPa) huff-n-puff recovery factors of the three gases at different GORs. As can be seen from Figure 6, the recovery factors of CO_2 and CH_4 increase with GOR; in terms of the three-gas average, the recovery factor rises from 6.7% at GOR 10 to 11.4% at GOR 20 and 15.5% at GOR 30. The recovery factor of flue gas is insensitive to GOR and remains low throughout.

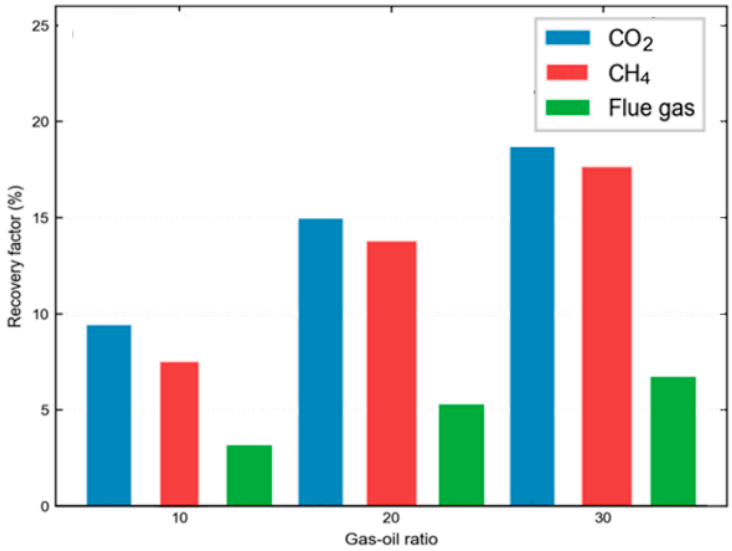


Figure 6. Effect of gas–oil ratio on the low-pressure stage (2 MPa) recovery factors of the three gases (120 °C).

A higher GOR corresponds to a larger amount of gas dissolved in the crude oil, so that during the low-pressure (solution gas) stage, the liberated gas produces a stronger volumetric expansion effect and a greater displacement energy. Within the tested range of GOR 10–30, the recovery factors of CO_2 and CH_4 increased monotonically with GOR, and no channeling-induced decline was observed; a decline is expected only once the GOR exceeds the channeling threshold, which lies beyond the tested window under the studied conditions. Gas channeling refers to the phenomenon whereby, during the soak stage, the excessively injected gas cannot fully dissolve and forms a free gas phase, which—during the depletion stage—preferentially breaks through along high-permeability channels, bypassing oil-bearing pores and producing a bypass effect. Because flue gas has inherently low solubility, most of the injected gas exists as a free gas phase and cannot be converted into effective displacement energy; therefore, its recovery factor is insensitive to GOR.

It can be concluded that, within the tested range, the recovery factor increased monotonically with GOR, so the optimum GOR lies at or above the upper bound of the tested window (GOR 30); this single-factor trend should be distinguished from the L9 result, in which the best-performing run (Run 4) includes the GOR 20 level, reflecting the level setting of the orthogonal design rather than a globally optimal GOR. A quantitative correlation of the optimum GOR with formation pressure and injection temperature will be developed in subsequent work. The present results indicate that GORs up to 30 do not induce gas channeling in extra-heavy oil systems at 30 MPa and 120 °C.

3.3.4. Effect of Viscosity Reducer Concentration on Recovery

Under the conditions of temperature 90 °C, GOR 30, and CO_2, the variations of the low-pressure stage (2 MPa) huff-n-puff recovery factor with viscosity reducer concentration were tested at four levels: 1, 3, 5, and 10 wt%. Because huff-n-puff with the viscosity reducer alone cannot proceed, the optimized gas CO_2 was retained in this group, and part of the CO_2 data served as the shared reference for the analysis.

Figure 7 shows the relationship between the low-pressure stage (2 MPa) huff-n-puff recovery factor and viscosity reducer concentration. As can be seen from Figure 7, when the viscosity reducer concentration is increased from 1 to 5 wt%, the recovery factor rises from 4.8% to 19.4% (an increase of 14.6 percentage points); when the concentration is further increased from 5 to 10 wt%, the recovery factor rises only to 21.3% (an increase of 1.9 percentage points), showing a clear pattern of diminishing marginal benefit. Correspondingly, the viscosity reduction rate already reaches 95.4% at 5 wt%, and further increases in concentration yield very limited improvement.

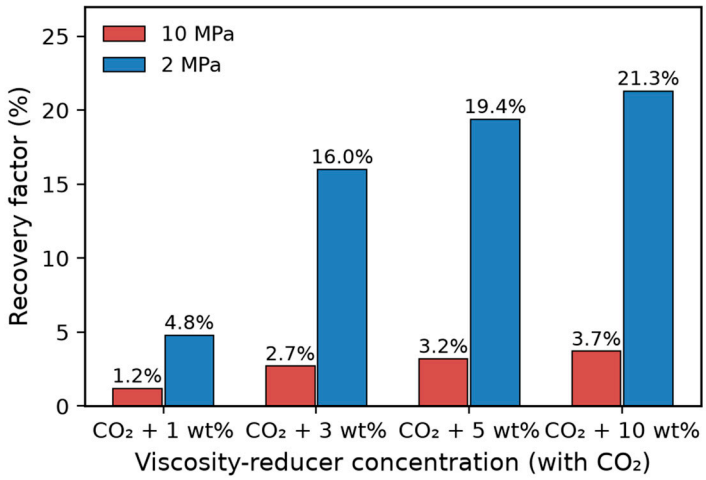


Figure 7. Effect of viscosity reducer concentration on the low-pressure stage (2 MPa) recovery factor.

A possible explanation for the diminishing incremental recovery beyond 5 wt% is that the adsorption of viscosity reducer molecules at the asphaltene/resin or oil–water interfaces approaches saturation, so that additional molecules contribute little to further dispersion improvement; however, no adsorption isotherm or interfacial measurements were performed, and this interpretation remains to be verified. Mechanistically, the viscosity reducer disrupts the π–π stacking and hydrogen-bonding network of asphaltene aggregates and inserts between resin–asphaltene molecules to weaken intermolecular forces, thereby lowering the apparent viscosity of the crude oil. However, the chemical agent acts only on the flow-capacity dimension and has no direct contribution to the solution gas driving force; therefore, simply increasing the viscosity reducer concentration cannot compensate for an insufficient gas source.

Hence, 5 wt% is identified as a practically preferred concentration within the tested range of 1–10 wt%, i.e., the concentration beyond which the incremental recovery benefit becomes limited, although the recovery factor at 10 wt% remained slightly higher. The viscosity reducer should be used in combination with the gas effect to balance recovery performance against chemical dosage.

3.3.5. MCTF Enhancement Mechanism and Best-Performing Conditions

An L9(3^4) orthogonal experimental design was adopted with four factors—injection temperature (90/120/150 °C), gas type (CO_2/CH_4/flue gas), GOR (10/20/30), and viscosity-

reducer concentration (0/3/5 wt%)—at three levels each, yielding a total of nine experiments; the results are shown in Figure 8. Run 4 (120 °C + CO_2 + GOR 20 + 5 wt% viscosity reducer) achieved the highest total recovery factor of 44.6%, outperforming the other eight groups, whereas Run 1 (90 °C + CO_2 + GOR 10, 0 wt% viscosity reducer) yielded the lowest total recovery factor of 15.2%. Unless otherwise indicated, the recovery factors of the single-factor experiments in Sections 3.3.1–3.3.4 refer to the low-pressure stage (2 MPa) recovery factor, whereas the recovery factors of the L9 orthogonal experiments refer to the total recovery factor over the whole depletion process (from the initial 30 MPa to the terminal 2 MPa).

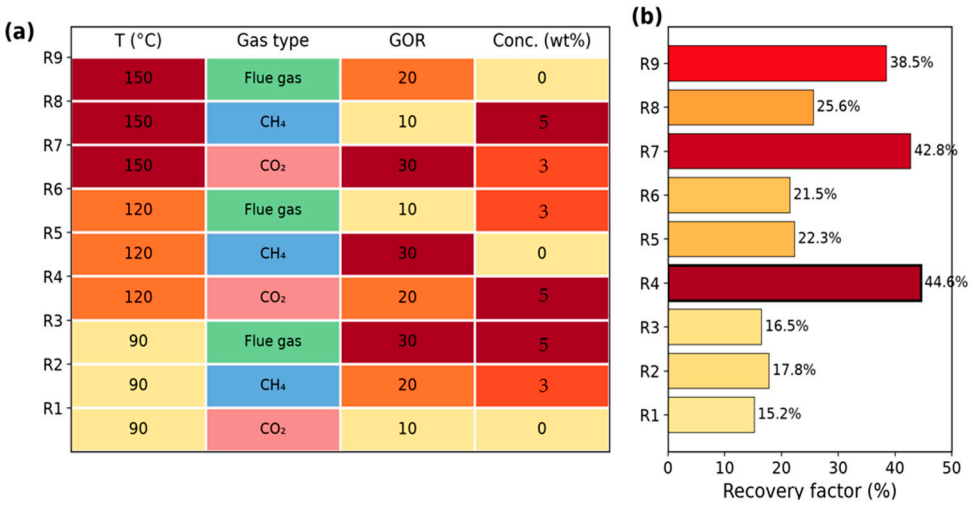


Figure 8. L9(3^4) orthogonal experimental design matrix and results. (**a**) Design matrix, with cell color encoding the recovery factor (YlOrRd); the gas type column is color-coded as CO_2 red/CH_4 blue/flue gas green; (**b**) corresponding total recovery factors ranked; Run 4 (120 °C + CO_2 + GOR 20 + 5 wt%) shows the highest total recovery factor of 44.6%.

The reason that Run 4 is markedly superior to the other conditions is that this combination simultaneously reaches favorable levels across all four factors: the temperature of 120 °C has already exceeded the Arrhenius rheological inflection point of the crude oil, fully releasing the thermal viscosity reduction effect; CO_2 at 30 MPa has a solubility of 114.9 m^3/m^3, which further improves crude oil mobility through dissolution-driven viscosity reduction while also reserving ample solution gas drive energy for the subsequent depletion production stage; the GOR of 20 provides a dissolved gas amount that matches the crude oil flow capacity, ensuring sufficient solution gas driving force in the low-pressure stage without inducing gas channeling; and the viscosity reducer concentration of 5 wt% corresponds to the level beyond which the incremental recovery becomes marginal, suggesting—but not directly demonstrating—an approach to adsorption saturation, since no adsorption isotherm was measured. By contrast, Run 1 is at a disadvantage in three of the four factors: the insufficient temperature (90 °C) prevents the crude oil from crossing the flow initiation threshold, the low GOR (10) provides scarce solution gas drive energy, and the absence of viscosity reducer eliminates the chemical viscosity reduction effect. Consequently, its recovery factor is only 15.2%.

Synthesizing the single-factor analysis results of Sections 3.3.1–3.3.4, the three components of the MCTF (hot water, gas, viscosity reducer) make differentiated contributions to the huff-n-puff recovery factor through different mechanisms: the hot water phase, by raising the temperature, disrupts the π–π stacking and van der Waals forces between asphaltene–resin molecules, lowers the crude oil viscosity, and improves oil phase mobility; CO_2, through dissolution-driven viscosity reduction, crude oil swelling, and solution gas

drive, both improves mobility and supplements the driving energy; and the viscosity reducer, through O/W emulsification and asphaltene dispersion, further lowers the apparent crude oil viscosity on top of thermal viscosity reduction. The mutual reinforcement among the three components (for example, the increase of the CO_2 diffusion coefficient with decreasing crude oil viscosity, or the effect of interfacial tension reduction on gas mass transfer) is physically plausible; however, such coupling effects cannot be quantified with the present dataset and would require strictly matched control experiments. Table 3 summarizes the linkage between each proposed mechanism and the experimental evidence that directly supports it, distinguishing direct observations from mechanistic interpretations.

Table 3. Linkage between the proposed mechanisms and the experimental evidence, distinguishing direct observations from mechanistic interpretations.

Mechanism	Direct Evidence (Measured)	Interpretation (Not Directly Measured)
Thermal	Viscosity–temperature curve and Arrhenius inflection at 120 °C (Figure 2); recovery factor vs. temperature (Figure 5)	Mobility gain outweighs solubility loss below 120 °C; residual oil limitation slows growth above it
Gas	PVT solubility and viscosity-reduction data (Figure 3); recovery ranking and GOR response (Figures 4 and 6)	Solubility order governs both flow capacity and driving energy
Chemical	Concentration–viscosity data; recovery factor vs. concentration (Figure 7)	Adsorption approaching saturation (unverified); acts on flow capacity only
Component interactions	L9 combined performance only (Figure 8); no matched control runs	Mutual reinforcement plausible but unquantified; separation requires matched control runs

Viewed across the single-factor experiments of Sections 3.3.1–3.3.4, the three components of the MCTF act on different aspects of the recovery process—the thermal effect mainly on crude oil mobility, the gas effect on both mobility and driving energy, and the chemical effect on mobility—so the combined system benefited from all three mechanisms. Because strictly matched control runs (e.g., reducer-free and gas-free counterparts at otherwise identical conditions) are not yet available, the contributions of the three components cannot be quantitatively decomposed; such controlled experiments are planned as subsequent work.

Therefore, among the nine tested orthogonal combinations, Run 4 (120 °C + CO_2 + GOR 20 + 5 wt% viscosity reducer) achieved the highest total recovery factor of 44.6%. This process achieves the best combined performance of the thermal, gas, and chemical effects among the tested runs; it does not demonstrate a global optimum, because the L9 design does not exhaust all four-factor combinations and the recovery factor increased monotonically over the tested GOR range of 10–30, so the optimum GOR lies at or above the tested upper bound. The qualitative analysis above indicates that the three components act through complementary mechanisms; quantitative characterization of the interactions among them cannot be achieved with the present data and would require additional strictly matched control experiments, which are planned as subsequent work.

3.3.6. Mechanistic Differences Among the Factors

The above experimental results indicate that the four factors have distinctly different effects on the crude oil recovery factor in terms of magnitude, sensitive range, and mode of action, reflecting differences in their underlying mechanisms. Grey relational analysis are shown in Figure 9. It was applied to process the data of the nine orthogonal experiments, yielding the grey relational ranking of the four factors: injection temperature (0.876) > viscosity reducer concentration (0.812) > gas type (0.754) > GOR (0.638). The grey relational

degree measures the degree of association between the normalized factor sequences and the recovery factor sequence; it is used here for factor screening and ranking only and does not represent an independent causal or variance contribution of each factor to the recovery factor. Injection temperature has the highest relational degree and is the primary controlling factor of huff-n-puff recovery; GOR has the lowest relational degree, and its response within the tested range was moderate and monotonic. The influence patterns of each factor are analyzed below from a mechanistic perspective. Grey relational analysis was selected over range analysis and analysis of variance because it is applicable to small samples (nine runs), requires no distributional assumptions, and ranks factors on a normalized interval scale; the grey relational degrees were computed with the recovery factor as the reference sequence, using interval normalization and a distinguishing coefficient of 0.5 [35,36].

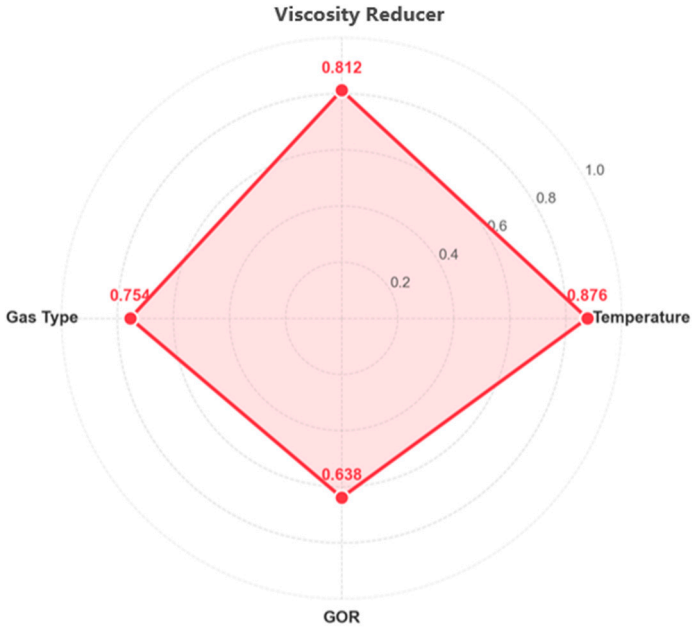


Figure 9. Radar chart of the grey relational degrees of the four factors (temperature 0.876, viscosity reducer concentration 0.812, gas type 0.754, GOR 0.638), derived from the nine-run L9 orthogonal experiments.

The dominant role of injection temperature is fundamentally attributable to the extreme sensitivity of extra-heavy oil viscosity to temperature. According to the viscosity–temperature data, increasing the temperature from 90 °C to 120 °C reduces the crude oil viscosity from 8.0×10^3 mPa·s at 90 °C to 7.8×10^2 mPa·s at 120 °C (90% decrease), transitioning the crude oil from a state of virtually no flow capability to one of effective flow. Piecewise Arrhenius fitting indicates that 120 °C is the rheological inflection point of the crude oil: the low-temperature segment (80–120 °C) has an activation energy of 78.5 kJ/mol, while the high-temperature segment (120–160 °C) has a reduced activation energy of 64.9 kJ/mol, indicating that high temperature disrupts the π–π stacking and van der Waals forces between asphaltene–resin molecules. Once the crude oil viscosity falls below a critical value, connected flow channels are established within the pore network, and a marked jump in the recovery factor occurs. The slowdown in recovery growth within 120–150 °C is not due to saturation of the temperature effect but rather because residual oil saturation becomes the new limiting factor—most of the mobile oil has already been mobilized at 120 °C.

As Figure 9 shown, the relational degree of viscosity reducer concentration (0.812) is slightly lower than that of temperature but markedly higher than those of the gas-related factors, indicating that chemical viscosity reduction provides substantial secondary reinforcement after thermal energy establishes the baseline viscosity reduction. The viscosity

reducer contributes a 14.6 percentage point recovery improvement over the concentration range of 1–5 wt%; however, its highly nonlinear behavior (5 wt% → 10 wt% contributes only a 1.9 percentage point increment) indicates a diminishing marginal benefit at higher concentrations; adsorption approaching saturation at the interface is a possible explanation, but no adsorption or interfacial tension measurements were performed to verify it.

As Figure 9 shown, the influence of gas type (relational degree 0.754) mainly originates from the difference in solubility between CO_2 and CH_4 in extra-heavy oil. The solubility of CO_2 is about three times that of CH_4 (about 120 m^3/m^3 vs. about 40 m^3/m^3 at 30 MPa and 90 °C), which can be explained at the molecular level: the kinetic diameter of CO_2 (0.33 nm) is smaller than that of CH_4 (0.38 nm), making it easier to insert between asphaltene–resin lamellae; the quadrupole moment of CO_2 enables stronger interactions with the polar components (resins and asphaltenes) of the crude oil than CH_4. At 30 MPa and 90 °C, CO_2 is already in a supercritical state (critical temperature 31.1 °C), combining the diffusivity of a gas with the dissolving power of a liquid, and its mass transfer efficiency is markedly higher than that of gaseous CH_4 [12,14]. The oil increment effect of CO_2 is about 1.5–2.0 times that of CH_4. Because gas is the sole source of solution gas driving force, the gas type effectively determines the upper limit of solution gas drive energy.

As Figure 9 shown, the relational degree of GOR is the lowest (0.638). Within the tested window (GOR 10–30), gas channeling was not encountered, and the response of the recovery factor to GOR was moderate and monotonic, consistent with its lowest relational degree. The influence of GOR is bidirectional: at too low a GOR, the dissolved gas amount is insufficient to form an effective drive, whereas at too high a GOR, gas channeling disrupts the flow field distribution. The optimal value is closely related to formation pressure, crude oil composition, and reservoir heterogeneity; under 30 MPa and 120 °C it lies at or above the tested upper bound (GOR 30) and will be refined in subsequent work.

3.3.7. Comparison with Published Studies on Other Heavy Oil Systems

Because all quantitative conclusions of this study are specific to the tested Shengli extra-heavy oil system, the present results are compared with published experiments on other heavy oil systems to delineate which trends are system-independent and which values are system-specific. The gas ranking observed here (CO_2 > CH_4 > flue gas) is consistent with the classical laboratory evaluation of CO_2 huff-n-puff in Lloydminster heavy oil by Sayegh and Maini [38], in which CO_2 dissolution produced strong viscosity reduction and CO_2 was retained preferentially to CH_4 during pressure depletion, and with the experiments of Wei et al. [39], in which CO_2 markedly outperformed N_2 in oil swelling, viscosity reduction, and hydrocarbon extraction for a Chinese heavy oil with an average viscosity of about 5000 mPa·s. The absolute recovery levels, however, are not directly transferable: the gas-assisted steam huff-n-puff of Wei et al. [39] produced more than 10% incremental oil over natural depletion, whereas the present MCTF tests yielded a total recovery factor of 44.6% at the best-performing combination under 30 MPa, reflecting differences in pressure regime, injected fluid composition, and crude oil system.

The multi-component thermal fluid route itself is supported by independent studies: Yu et al. [40] reported that MCTF huff-n-puff improved oil recovery by 9.68% over pure steam in offshore heavy oil simulations accounting for reservoir damage, and the Bohai offshore pilot documented by Liu et al. [6] has operated MCTF huff-n-puff since 2008, confirming the engineering viability of the combined thermal–gas process that the present experiments quantify in the laboratory. The chemical route shows the same trend-level agreement: the anion–nonionic surfactant system used here is consistent with the viscosity reduction and emulsification behavior reported for anion–nonionic surfactants on other heavy crudes [15], and the 6–16% incremental recovery factors obtained with surfactant–

steam processes by Zeidani and Gupta [22] are of the same order as the 14.6 percentage point gain observed over 1–5 wt% in the present tests, although the two processes are not identical.

At the same time, the quantitative differences among these studies are substantial. The optimal gas/steam ratio (about 9.4 cm^3/cm^3) reported by Bagci and Gümrah for gas–steam co-injection [8] is defined differently from the GOR used here (gas volume per oil volume at standard conditions), so the two windows cannot be compared numerically; likewise, the preferred injection temperature and the diminishing marginal benefit concentration observed here (120 °C and approximately 5 wt%) reflect the viscosity–temperature characteristics and composition of the tested Shengli crude and should not be extrapolated to other systems without re-evaluation. These comparisons reinforce the scope limitation stated throughout this work: the trends (temperature dominance, CO_2 superiority, and chemical diminishing returns) are consistent across heavy oil systems, whereas the quantitative values are specific to the present system and conditions.

4. Conclusions

Based on one-dimensional sand pack high-pressure (30 MPa) depletion huff-n-puff experiments and the accompanying viscosity–temperature, PVT, and viscosity reducer concentration tests, this study systematically investigates the enhancement mechanism of MCTF huff-n-puff in deep extra-heavy oil from the new perspective of "flow-capacity vs. driving-energy balance". The main conclusions are as follows:

(1) The final recovery factor of MCTF huff-n-puff is jointly determined by two dimensions: the crude oil flow capacity and the solution gas driving force. The former is dominated by temperature and the viscosity reducer, whereas the latter is dominated by gas solubility and GOR. The two-stage decomposition of the depletion production process (high-pressure elastic drive + low-pressure solution gas drive) provides an experimental means of decoupling these two dimensions. The low-pressure stage (2 MPa) is the dominant production period, and its recovery factor is jointly controlled by the coupled flow capacity and solution gas driving force.

(2) The three components of the MCTF exhibit differentiated contributions to the two dimensions: the thermal effect dominates flow capacity but has the side effect of weakening the driving energy; the gas effect contributes to both flow capacity and driving energy (it is the only component that contributes to driving energy); and the chemical effect is dedicated solely to flow capacity (with no direct contribution to driving energy). This differentiated positioning is the physical basis of the joint enhancement. Specific data: thermal viscosity reduction 98.7%; CO_2 viscosity reduction 97.6% with solubility 114.9 m^3/m^3; viscosity reducer viscosity reduction 95.4% (5 wt% is the concentration beyond which the incremental benefit diminishes within the tested range of 1–10 wt%; adsorption saturation is a possible but unverified explanation).

(3) The highest total recovery factor among the nine orthogonal experiments, 44.6%, was obtained at 120 °C + CO_2 + GOR 20 + 5 wt% viscosity reducer; within the tested design, this combination simultaneously achieved favorable levels of the four factors (temperature past the rheological inflection point, CO_2 as the preferred gas medium, GOR at the best-performing level without gas channeling, and 5 wt% as the concentration beyond which the incremental benefit diminishes). The reported combination represents the best-performing condition within the tested experimental range and system (one-dimensional sand pack model, 30 MPa, and the tested Shengli extra-heavy oil system); further validation is required before extrapolation to field conditions.

(4) The grey relational ranking of the four factors is: injection temperature (0.876) > viscosity reducer concentration (0.812) > gas type (0.754) > GOR (0.638). Within the

present dataset, this ranking is a data-based ordering of the four factors under the tested conditions and should not be over-interpreted: the first place of injection temperature is consistent with the one-to-two order of magnitude viscosity reduction observed over 90–150 °C (Figure 2) and with the recovery increase over 90–120 °C (Figure 5); the rank of the viscosity reducer concentration is consistent with the 14.6 percentage point gain over 1–5 wt% (Figure 7); and the lowest rank of GOR is consistent with its moderate, monotonic response within the tested window (Figure 6). The grey relational degrees provide a screening-level ranking and do not represent independently verified causal contributions of the factors.

Future research directions include conducting multi-cycle huff-n-puff experiments in three-dimensional physical models to evaluate the cycle evolution law of the balance and coupling CMG STARS numerical simulation to achieve scale-up from one-dimensional experiments to three-dimensional reservoirs.

Supplementary Materials: The following supporting information can be downloaded at: https://www.mdpi.com/article/10.3390/pr14213537/s1. Table S1: Complete experimental matrix of all independently conducted sand-pack experiments.

Author Contributions: Conceptualization, R.H., T.L. and R.S.; methodology, J.Z.; software, Z.Y. and R.S.; validation, R.H., R.S., Z.Y. and M.W.; formal analysis, L.M.; investigation, M.W.; resources, Z.Y., X.W. and H.Z.; data curation, R.H.; writing—original draft preparation, R.H. and R.S.; writing—review and editing, B.L. and Z.Z.; visualization, H.Z.; supervision, X.W.; project administration, M.W.; funding acquisition, T.L. and B.L. All authors have read and agreed to the published version of the manuscript.

Funding: This work was financially supported by Science Project of COSL. (E-23257011) and Tianjin International Cooperation Project (25YFGKHZ00220).

Data Availability Statement: The original contributions presented in this study are included in the article/Supplementary Material. Further inquiries can be directed to the corresponding author.

Acknowledgments: We are grateful to the Shandong Engineering Research Center for CO_2 Utilization and Storage for their kind help in this study. The valuable comments made by the anonymous reviewers are also sincerely appreciated.

Conflicts of Interest: Authors Rui Han, Tao Lin, Jianliang Zhang were employed by the National Key Laboratory for Efficient Development of offshore Oil and Gas. Authors Rui Han, Tao Lin, Jianliang Zhang, Rong Sun, Zhongtao Yuan, Ming Wang, and Lan Mo were employed by the Key Laboratory of Offshore Heavy Oil Thermal Recovery, China National Offshore Oil Corporation Limited. Authors Rong Sun and Zhongtao Yuan, Ming Wang, and Lan Mo were employed by the China Oilfield Services Limited. The remaining authors declare that the research was conducted in the absence of any commercial or financial relationships that could be construed as a potential conflict of interest. The authors declare that this study received funding from the China Oilfield Services Limited. The funder had no role in designing the study; in the collection, analyses, or interpretation of data; in the writing of the manuscript; or in the decision to publish the results.

References

1. *SY/T 6165-1995*; Reservoir Classification; Standard of Petroleum and Natural Gas Industry of China. Petroleum Industry Press: Beijing, China, 1995. (In Chinese)
2. Luo, P.; Gu, Y. Effects of asphaltene content on the heavy oil viscosity at different temperatures. *Fuel* **2007**, *86*, 1069–1078. [CrossRef]
3. Cheng, H.Z.; Chen, J.W.; Sun, R.Y.; Li, D.X. Effect of dissolved carbon dioxide on the viscosity of crude oil. *J. Univ. Pet. China* **2004**, *28*, 78–80. (In Chinese)
4. Bera, A.; Babadagli, T. Status of electromagnetic heating for enhanced heavy oil/bitumen recovery and future prospects: A review. *Appl. Energy* **2015**, *151*, 206–226. [CrossRef]

5. Wang, X. Heavy oil recovery techniques in Liaohe Oilfield and key technical research in next step. *Pet. Explor. Dev.* **2006**, *33*, 484–490. (In Chinese)
6. Liu, Y.; Zou, J.; Meng, X.; Han, X.; Sun, Y.; Zhang, W.; Zhou, F.; Fang, J. Treatment technology of steam breakthrough for offshore heavy oil reservoirs developed by huff and puff with multi-component thermal fluid. In Proceedings of the SPE Asia Pacific Enhanced Oil Recovery Conference, Kuala Lumpur, Malaysia, 11–13 August 2015; p. SPE-174703-MS. [CrossRef]
7. Du, Y.; Wang, Y.; Jiang, P.; Ge, J.; Zhang, G. Mechanism and feasibility study of nitrogen assisted cyclic steam stimulation for ultra-heavy oil reservoir. In Proceedings of the SPE Enhanced Oil Recovery Conference, Kuala Lumpur, Malaysia, 2–4 July 2013; p. SPE-165212-MS. [CrossRef]
8. Bagci, S.; Gümrah, F. An investigation of noncondensable gas–steam injection for heavy oil recovery. In Proceedings of the 8th European Symposium on Improved Oil Recovery, Vienna, Austria, 15–17 May 1995. [CrossRef]
9. Dong, X.H.; Liu, H.; Chen, Z.; Wu, K.; Lu, N.; Zhang, Q. Enhanced oil recovery techniques for heavy oil and oilsands reservoirs after steam injection. *Appl. Energy* **2019**, *239*, 1190–1211. [CrossRef]
10. Sheng, J.J. Enhanced oil recovery in shale reservoirs by gas injection. *J. Nat. Gas Sci. Eng.* **2015**, *22*, 252–259. [CrossRef]
11. Zhou, X.; Yuan, Q.; Peng, X.; Zeng, F.; Zhang, L. A critical review of the CO_2 huff 'n' puff process for enhanced heavy oil recovery. *Fuel* **2018**, *215*, 813–824. [CrossRef]
12. Song, C.; Yang, D. Experimental and numerical evaluation of CO_2 huff-n-puff processes in Bakken formation. *Fuel* **2017**, *190*, 145–162. [CrossRef]
13. Sweatman, R.E.; Parker, M.E.; Crookshank, S.L. Industry experience with CO_2-enhanced oil recovery technology. In Proceedings of the SPE International Conference on CO_2 Capture, Storage, and Utilization, San Diego, CA, USA, 2–4 November 2009; p. SPE-126446-MS. [CrossRef]
14. Li, H.B.; Yang, D.Y. Experimental and theoretical determination of equilibrium interfacial tension for the solvent(s)-CO_2-heavy oil systems. *Energy Fuels* **2012**, *26*, 1776–1786. [CrossRef]
15. Si, Y.; Zhu, Y.; Liu, T.; Xu, X.; Yang, J. Synthesis of a novel borate ester anion–nonionic surfactant and its application in viscosity reduction and emulsification of heavy crude oil. *Fuel* **2023**, *333*, 126453. [CrossRef]
16. Shi, W.; Ma, Y.; Tao, L.; Zhang, N.; Ma, C.; Bai, J.; Xu, Z.; Zhu, Q.; Zhong, Y. Study of the enhanced oil recovery mechanism and remaining oil state of heavy oil after viscosity-reducer-assisted CO_2 foam flooding: 2D microvisualization experimental case. *Energy Fuels* **2023**, *37*, 18620–18631. [CrossRef]
17. Li, Z.M.; Lu, T.; Tao, L.; Li, B.; Zhang, J.; Li, J. CO_2 and viscosity breaker assisted steam huff and puff technology for horizontal wells in a super-heavy oil reservoir. *Pet. Explor. Dev.* **2011**, *38*, 600–605. (In Chinese) [CrossRef]
18. Liu, W.; Li, Z. The effect of the elements in HDCS technology on the properties of super heavy oil. *Spec. Oil Gas Reserv.* **2013**, *20*, 127–130. (In Chinese)
19. Liu, W.; Du, L.; Zou, X.; Liu, T.; Wu, X.; Wang, Y.; Dong, J. Experimental study on the enhanced ultra-heavy oil recovery using an oil-soluble viscosity reducer and CO_2 assisted steam flooding. *Geoenergy Sci. Eng.* **2023**, *222*, 211409. [CrossRef]
20. Liu, Y.L.; Zhang, C.; Li, S.-Y.; Li, Z.-M. Study of steam heat transfer enhanced by CO_2 and chemical agents in heavy oil production. *Pet. Sci.* **2023**, *20*, 1030–1043. [CrossRef]
21. Sun, J.F. Adaptability evaluation of surfactant assisted steam flooding for heavy oil reservoir. *Oilfield Chem.* **2012**, *29*, 60–64. (In Chinese)
22. Zeidani, K.; Gupta, S.C. Surfactant-steam process: An innovative enhanced heavy oil recovery method for thermal applications. In Proceedings of the SPE Heavy Oil Conference, Calgary, AB, Canada, 11–13 June 2013; p. SPE-165545-MS.
23. Zhao, X.T.; Bai, Y.R.; Han, S.B.; Wang, X.P. Advances in improving heavy oil recovery by thermochemical techniques. *Spec. Oil Gas Reserv.* **2012**, *19*, 8–13. (In Chinese)
24. Wu, Z.B.; Liu, H.; Wang, X. Adaptability research of thermal-chemical assisted steam injection in heavy oil reservoirs. *J. Energy Resour. Technol.* **2018**, *140*, 052901. [CrossRef]
25. Liu, Z.P.; Li, Z.M. An experimental study on anti-channeling technology with foam in CO_2 flooding. *J. Southwest Pet. Univ.* **2015**, *37*, 117–122. (In Chinese)
26. Feng, Y.J. Molecular simulation and its application in the oilfield chemistry and related fields. *Oilfield Chem.* **1998**, *15*, 71–76. (In Chinese)
27. Ji, B.Y.; Fang, J.; Yang, S.; Hu, Y. Concept, method and prospect of molecular oil recovery. *Oil Gas Geol.* **2023**, *44*, 195–202. (In Chinese)
28. Zhang, H.; Yuan, S.L. Application of molecular dynamics simulation in enhanced oil recovery. *Sci. Sin. Chim.* **2021**, *51*, 761–771. [CrossRef]
29. Zhao, Q.Y.; Zheng, L.; Dong, Y.; Jin, H.; Wang, Y.; Guo, L. Molecular dynamics simulation of heavy oil dissolution in supercritical water and multicomponent thermal fluid. *Sustain. Energy Fuels* **2023**, *7*, 4094. [CrossRef]

30. Lu, N.; Dong, X.; Wang, H.; Liu, H.; Chen, Z.; Li, Y.; Zeng, D. Hybrid CO_2 thermal system for post-steam heavy oil recovery: Insights from microscopic visualization experiments and molecular dynamics simulations. *Energy Geosci.* **2025**, *6*, 100394. [CrossRef]
31. Smith, G.E. Fluid flow and sand production in heavy-oil reservoirs under solution-gas drive. *SPE Prod. Eng.* **1988**, *3*, 169–180. [CrossRef]
32. Maini, B.B. Foamy oil flow in primary production of heavy oil under solution gas drive. In Proceedings of the SPE Annual Technical Conference and Exhibition, Houston, TX, USA, 3–6 October 1999; p. SPE-56541.
33. Pooladi-Darvish, M.; Firoozabadi, A. Solution-gas drive in heavy oil reservoirs. *J. Can. Pet. Technol.* **1999**, *38*, 54–61. [CrossRef]
34. Pooladi-Darvish, M.; Okazawa, T. Effect of depletion rate on gas mobility and solution gas drive in heavy oil. *SPE J.* **2002**, *7*, 213–220. [CrossRef]
35. Deng, J.L. Introduction to grey system theory. *J. Grey Syst.* **1989**, *1*, 1–24. [CrossRef]
36. Zhang, H.; Wang, J.; Zhang, H. Investigation of the main factors during shale-gas production using grey relational analysis. *Open Pet. Eng. J.* **2016**, *9*, 207–215. [CrossRef]
37. Sun, J. Experimental study on single-phase flow characteristics of ultra-heavy oil in the Zheng411 block, Shengli Oilfield. *Pet. Drill. Tech.* **2011**, *39*, 86–90. (In Chinese) [CrossRef]
38. Sayegh, S.G.; Maini, B.B. Laboratory evaluation of the CO_2 huff-n-puff process for heavy oil reservoirs. *J. Can. Pet. Technol.* **1984**, *23*, 29–36. [CrossRef]
39. Wei, B.; Pang, S.; Pu, W.; Lu, L.; Wang, C.; Kong, L. Mechanisms of N_2 and CO_2 assisted steam huff-n-puff process in enhancing heavy oil recovery: A case study using experimental and numerical simulation. In Proceedings of the SPE Middle East Oil & Gas Show and Conference, Manama, Bahrain, 6–9 March 2017; p. SPE-183871-MS. [CrossRef]
40. Yu, X.; Liu, X.; Chen, M.; Wu, G.; Li, X. Study on influence of heavy oil reservoir damage caused by multi-component thermal fluid huff and puff. *Front. Energy Res.* **2022**, *10*, 821221. [CrossRef]

Disclaimer/Publisher's Note: The statements, opinions and data contained in all publications are solely those of the individual author(s) and contributor(s) and not of MDPI and/or the editor(s). MDPI and/or the editor(s) disclaim responsibility for any injury to people or property resulting from any ideas, methods, instructions or products referred to in the content.